Enhancement of physical properties of stain-etched porous silicon by integration of WO3 nanoparticles

M. Alaya, R. Benabderrahmane Zaghouani, S. Khamlich, J. -L. Lazzari, W. Dimassi

Enhancement of physical properties of stain-etched porous silicon by integration of WO3 nanoparticles

M. Alaya, R. Benabderrahmane Zaghouani, S. Khamlich, J.-L. Lazzari, W. Dimassi

PII: S0040-6090(17)30803-9
DOI: doi:10.1016/j.tsf.2017.10.041
Reference: TSF 36309

To appear in: *Thin Solid Films*

Received date: 15 December 2016
Revised date: 18 October 2017
Accepted date: 19 October 2017

Please cite this article as: M. Alaya, R. Benabderrahmane Zaghouani, S. Khamlich, J.-L. Lazzari, W. Dimassi , Enhancement of physical properties of stain-etched porous silicon by integration of WO3 nanoparticles. The address for the corresponding author was captured as affiliation for all authors. Please check if appropriate. Tsf(2017), doi:10.1016/j.tsf.2017.10.041

Enhancement of physical properties of stain-etched porous silicon by integration of WO_3 nanoparticles

M. Alaya[1], R. Benabderrahmane Zaghouani[1*], S. Khamlich[2], J.-L. Lazzari[3], W. Dimassi[1]

[1]*Laboratoire de Photovoltaïque, Centre de Recherches et des Technologies de l'Energie,Technopôle de Borj-Cédria, BP, 95 Hammam-Lif, Tunis, Tunisie*

[2]*iThemba LABS-National Research Foundation (NRF),PO Box 722, Somerset West 7129, South Africa*

[3]*Aix Marseille Université, CNRS, CINaM UMR 7325,*
Campus de Luminy, Case 913, 163, Avenue de Luminy, 13288 Marseille Cedex 09, France

[*]Corresponding author: Rabia Benabderrahmane
Tel.:+216 25639377; Fax: +216 79325825
E-mail address: rabia.benabderrahmane@gmail.com

Abstract

In this work, we report on the passivation of porous silicon (PS) by tungsten trioxide (WO_3) nanostructured thin films deposited via dip-coating of PS in tungsten hexachloride and water/ethanol solution. Structural analysis by Fourier transform infrared spectroscopy showed a partial disappearance of SiH_x and Si-O-Si peaks after WO_3 thin film deposition on the PS due to the replacement of H atoms by WO_3. Additionally, PS/WO_3 sample revealed weakly intense peaks which can be ascribed to O-W-O and W=O bridging bonds. Morphological analysis by atomic force spectroscopy showed the coverage of the PS surface by a nanostructured thin film of dense WO_3 nanoparticles with a size ranging from 40 to 60 nm. The photoluminescence signal intensity of PS/WO_3 samples presents a continuous increase as a function of the immersion time in the precursor solution. This is attributed to a better decoration of the PS surface by WO_3 nanoplatelets and a decrease of surface recombination velocity (200 x 10^2 cm/s for untreated silicon, 137 x 10^2 cm/s for PS and 99 x 10^2 cm/s for PS/WO_3samples). Hence, a ~ 50 % improvement in the effective lifetime of minority carriers is obtained. Moreover, the deposited WO_3 contributed not only to the passivation of PS, but acted as an antireflection layer which enhanced the optical properties of PS by reducing the reflection of light. These obtained results confirmed the benefits of using WO_3 thin film as passivation/antireflection coating for possible solar cell application.

Keywords: Porous silicon; Passivation; Tungsten oxide; Photoluminescence; Surface recombination velocity; Minority carrier lifetime.

1. Introduction

Although silicon being the dominant and mature material in the manufacturing of photovoltaic modules, there is a permanent quest for high-volume, high-throughput and cost-effectiveness coating technologies with multilayered materials having different functionalities. Indeed, transparency, conductivity, impermeability, photocatalytic [1], electrochromic, photochromic, passivation and antireflection properties are among those that could be combined in such multifunctional materials. In addition to the progress of coating technologies, the extension of nanotechnologies and the discovery of new nanostructuration processes have generated much interest. The nanostructuration of silicon have paved the way for different applications in microelectronic, photonic, photocatalysis [2-4], gaz sensors [5, 6] and photovoltaic devices [7]. Recent studies demonstrated that the quantum confinement of carriers in nanostructured silicon contributed to the efficiency enhancement when integrated in solar cells [8, 9]. Even if the silicon emits weak infrared photoluminescence due to its indirect band gap, the finding of a high visible photoluminescence from electrochemical etched silicon (porous silicon) [10, 11] was well exploited by the photovoltaic community [12]. Although largely debated, this discovery was attributed to quantum size crystalline structures [10]. In addition to its photoluminescence, porous silicon (PS) acts as an antireflection layer with a surface reflectance attaining less than 10% in the visible spectrum due to the light-trapping into its nano-pores. Porous silicon can be elaborated by different methods with a formation mechanism leading to H-terminated surface which is unstable in ambient conditions [12]. Particularly, the appearance of dangling bonds on PS surface when subjected to an atmospheric oxidation leading to a deterioration of PS electronic and optical properties, specially, the minority carrier lifetime and the photoluminescence signal. In silicon-based solar cells, to obtain the maximum of current, photo-generated carriers diffusing to metallic contacts should have a high diffusion length and then a high lifetime. Many researchers have demonstrated the necessity of a porous silicon passivation step in order to achieve PS stability before its integration in final devices [13]. Several materials used as PS passivation layer are reported in the literature. Ben Rabha *et al.* [14] reported porous silicon passivation by means of Al_2O_3 films of different thicknesses deposited by pulsed laser deposition technique. They found an enhancement of minority carrier lifetime in p-type monocrystalline silicon form 2 µs to 7 µs. In the same line, Du *et al.* demonstrated the improvement of PS photoluminescence (PL) properties (PL intensity and stability) by depositing a silica film by sol-gel method [15]. These results are explained by the formation of stable surface bonds by the oxidation of Si-H bonds. Raypah *et al.* reported also the passivation of electrochemical etched silicon by a thin silver layer using RF sputtering technique [16]. They obtained an improvement of PS photoluminescence. However, the reflectance of PS has been increased with silver deposition. On the other hand, zinc oxide is also used to enhance porous silicon properties. Indeed, Salman *et al.* had shown an enhancement of solar cells efficiency with ZnO/PS as antireflection layer [17]. Other materials have recently proved their effectiveness to passivate silicon and improve solar cells efficiency such as silicon carbide [18] and alumina [19].

To improve the PS properties, this work covers the use of tungsten oxide (WO_3) as passivation layer. This oxide is known as a semi-conductor with a band gap around 3 eV and good chemical stability in aqueous solutions. This binary material has attracted considerable attention for its outstanding electrochromic, photochromic and photocatalytic properties [20-22]. There have been tremendous reports on the use of metal-oxide-semi-conductor structures as gas sensors. In this context, the majority of the applications adopted WO_3 as sensing material due to its high sensitivity and stability. Most of the recent publications studied the properties of WO_3 under different

gases such as NO_2 [23]. WO_3 thin films could be synthesized by different physical and chemical methods such as: chemical vapor deposition [20, 24], spray pyrolysis [25], sol gel [26], electrodeposition [27, 28] and atomic layer deposition (ALD) [29]. Its properties are motivating and encouraging to use it in photovoltaic devices. This work highlights an original study with a focus on the improvement of porous silicon electronic and optical properties by passivation with WO_3 thin layers deposited by a dip-coating method. A specific emphasis was put on the improvement of the PS photoluminescence signal in addition to the increase of minority carrier lifetime by depositing WO_3 thin layers.

2. Experimental techniques

To synthesis porous silicon, solar grade boron-doped single crystalline silicon (100) substrates (Czochralski) with a resistivity of ~1-3 Ω.cm and a thickness of 200 µm were used. Before PS elaboration, silicon substrates were cleaned with boiling acetone for 10 min, followed by immersion in ethanol for 5 min and rinsed after that in deionized water in order to eliminate organic greases. Finally, the substrates were etched in 10 % hydrofluoric acid for 1 min to eliminate native oxide, rinsed in deionized water and dried with nitrogen flux. Porous silicon was formed by "stain etching" in a solution of hydrofluoric acid (40 wt %), nitric acid (65 wt %) and deionized water (HF: HNO_3: H_2O) = (1:2:3) in volumetric ratio for 2 min. Immediately, after formation of PS layer, the substrates were dip-coated in a solution containing tungsten hexachloride (WCl_6) prepared previously in order to deposit WO_3 layers [30]. WCl_6 was mixed with ethanol (50 %) and water (50 %) under stirring at ambient temperature for 3 hours, leading to a blue solution. The latter solution was stored in air for 7 days until the blue color disappears and then it is ready to be used.

In order to study the effect of WO_3 layers deposition on PS properties, the WCl_6 solution concentration and immersion times (t_{imm}) were varied. First, the morphological features of porous silicon before and after WO_3 treatment were characterized by a digital instrument, Nanoscope 3100 Atomic Force Microscopy (AFM) operating in tapping mode. WO_3 deposition was also studied by a Fourier Transform Infrared (FTIR) Nicolet MAGNA-IR 560 Spectrometer. The optical properties of the prepared samples based on the surface reflectivity were analyzed using PerkinElmer Lambda 950 UV/VIS. Photoluminescence (PL) analyses were performed at ambient temperature with a 447 nm excitation laser. Finally, the minority carrier's lifetime was measured by the "Sinton WCT-120 lifetime tester" in the quasi-steady-state mode. The measurement was based on the recombination dynamics of optically generated carriers. The excess carrier density was evaluated via inductively measured photoconductance signal. The minority carrier lifetime was determined by measuring simultaneously the photoconductance variation in the sample and the generation rate. The carrier lifetime was then presented as a function of the excess carrier density.

3. Results and discussion

3.1. Structural and morphological Studies of the deposited WO_3 on PS

FTIR analysis was performed on freshly prepared PS and PS/WO_3 samples. The FTIR absorption spectra are presented in Fig.1 (a). The principal recorded vibration bands observed for the two spectra are SiH_x stretching mode at 2112 cm^{-1}, Si-O-Si stretching mode at 1092 cm^{-1} and SiH_2 scissors mode at 907 cm^{-1}. Absorption bands

at 628 cm^{-1} and 672.7 cm^{-1} corresponding to Si-Si stretching mode and SiH_n (n=1and n=2) wagging mode were also observed. Moreover, the appearance of a peak at 861 cm^{-1} was attributed to the O-SiH_x wagging mode. We clearly noticed a reduction of SiH_x and Si-O-Si peaks intensity for PS/WO_3 sample, suggesting the replacement of H atoms by WO_3 entities [31]. In order to determine precisely the different W–O bands in the spectral region (400 cm^{-1}-1000 cm^{-1}), we have zoomed at different zones on the FTIR spectra of PS and PS/WO_3 samples. We observed appearance and disappearance of some peaks in the FTIR spectrum after a successful deposition of WO_3 nanostructured thin film. Fig.1 (b) and Fig.1 (c) show the amplification of zone 2 in PS and PS/WO_3 samples, respectively. After deconvolution of the large peak around 906 cm^{-1}, we obtained new peaks for PS/WO_3 sample at 927.7 cm^{-1} and 898.9 cm^{-1} corresponding to W═O and W-O-W bridging modes respectively [32,33]. In the PS FTIR spectrum, peaks situated at 962.5 cm^{-1} and 934.9 cm^{-1} disappeared. After amplification of zone 3 and deconvolution (Fig.1 (d) and Fig.1 (e)), a band at 782.9 cm^{-1} attributed to W–O_{intra}–W bridging stretch mode was easily distinguished [34], other peak situated at 802 cm^{-1} was clearly disappeared.

The surface topography of the untreated PS was investigated by AFM, and the 2D micro-image was depicted in Fig. 2(a). After immersion in a WCl_6 solution, porous silicon surface was totally covered with nanostructured features of WO_3 (Fig. 2(b)). Quasi-spherical WO_3 nanoparticles with a 60 nm in average size were clearly observed when the immersion time of 360 s in WCL_6 solution was used; this was confirmed by the top-view SEM image of treated PS sample as shown in Fig. 2(c).

3.2. WO_3 nanostructured thin film influence on the PS physical properties

3.2.1. Surface reflectivity

Fig. 3 (a) shows the surface reflectivity of PS and PS/WO_3 samples at different immersion times (30 s, 90 s, and 120 s) in a WCl_6 solution of 0.086 mol/L concentration. PS sample presents a reflectivity of about 5 % in the visible spectral region. This low reflectivity compared to the bare silicon (Fig.3 (b)) is attributed to light trapping in the porous surface of PS. This interesting property of PS must be conserved when performing any chemical or physical treatment of the PS surface. Having a low reflectivity, in particular around the UV-VIS region of the solar spectrum, an efficient photovoltaic device could be fabricated [35]. As can be seen in Fig. 3 (a), WO_3 deposition leads to a reflectance decrease as regard to PS sample, specifically between 250 nm and 550 nm of the spectral region.

3.2.2. Minority carrier lifetime

As mentioned above, the mechanism of porous silicon formation leads to a discontinuity in silicon crystal structure, which directly results in large density of dangling bonds at its surface giving rise to a high density of recombination-active defect levels. The impact of these interface defects on electrical porous silicon properties depends on their density, their capture cross section and their energy levels. The surface recombination is directly quantified by the surface recombination velocity S as given in the (Eq.1) [36]:

$$S = \frac{U_s}{\Delta n} \qquad \text{(Eq.1)}$$

Where U_s is the surface recombination rate and Δn is the excess carrier density. The determination of S permits the quality evaluation of the surface passivation, which reduces surface recombination effect by optimizing the interface properties. In this work, porous silicon is passivated by a thin layer of tungsten oxide. FTIR results

revealed the presence of W atoms. These atoms are filling the dangling bonds and changing the interface which result in a change in the defect properties. The reduction of the interface trap density and the capture cross section results in the reduction of the surface recombination rate, and so to the decrease of the surface recombination velocity. Consequently, with WO_3 deposition, the increasing of the effective minority carrier lifetime τ_{eff} in the porous silicon samples is expected. The minority carrier lifetime is measured using the WCT-120 photoconductance lifetime tester in the quasi-steady-state mode (QSSPC). The τ_{eff} takes into account the impact of the different bulk recombination channels and also the surface recombination. These different mechanisms may occur simultaneously in the same sample. The τ_{eff} is provided by (Eq.2):

$$\frac{1}{\tau_{eff}} = \frac{1}{\tau_{bulk}} + \frac{1}{\tau_{surface}} \qquad \text{(Eq.2)}$$

In the surface minority carrier lifetime term, the back and front surface contributions are considered:

$$\frac{1}{\tau_{surface}} = \frac{1}{\tau_{front-surface}} + \frac{1}{\tau_{back-surface}} \qquad (3)$$

In this work, back and front surfaces are identically passivated (S_1=S_2= S). τ_{eff} is then expressed by:

$$\frac{1}{\tau_{eff}} = \frac{1}{\tau_{bulk}} + \frac{2S}{w} \qquad (4)$$

Where w is the sample thickness.

In order to optimize the deposition parameters, we have varied WO_3 solution concentration and measured τ_{eff} for different immersion times. We prepared three different concentrations: C_1=0.086 mol/L, C_2= 0.035 mol/L and C_3= 0.018 mol/L. In Fig. 4, the evolution of the minority carrier lifetime as a function of excess carrier density Δn for the concentrations C_1, C_2 and C_3 with a deposition time of 30 s is reported. Porous silicon sample, freshly prepared, has an H-terminated surface. Consequently, minority carrier lifetime is greater in PS sample than in silicon substrate. Comparing PS and PS/WO_3 samples for the different concentrations, we observed that almost the same τ_{eff} for C_1 and C_2 was obtained. This behavior can be explained by the increase of WCl_6 solution viscosity at relatively high concentrations. WO_3 may not diffuse into the PS structure forming a glass layer and doesn't passivate PS surface defects. So, we have decreased the solution concentration and as we can observe for C_3 τ_{eff} is increased. In Fig. 5 (a), we notice an enhancement in the effective carrier lifetime as the immersion time increases for the concentration C_3. This is attributed to defects passivation and so to the decrease of the surface recombination velocity S. This velocity can be obtained via the following equation:

$$S = \frac{w}{2}\left(\frac{1}{\tau_{eff}} - \frac{1}{\tau_{bulk}}\right) \qquad (5)$$

To calculate bulk lifetime (τ_{bulk}), the surface recombination must be reduced until we can consider that the measured effective lifetime reflects the bulk recombination contribution. This is possible by passivating the surfaces. In this work, a bare silicon sample was chemically passivated using Iodine–Ethanol solution [37]. Silicon sample was covered on both sides with Iodine–Ethanol solution, placed in a transparent bag and measured with the Sinton WCT-120 lifetime tester giving a bulk minority carrier lifetime of the order of 19 µs.

The passivation mechanism was explained in details previously [37]. Fig.5 (b) depicts the surface recombination velocity S for silicon, PS and PS/WO_3 samples. It can be noted that a significant reduction of S from 137.5 x10^2 cm/s for porous silicon sample to 94.4x10^2 cm/s for PS/WO_3 sample with an immersion time of 360 s. These results confirmed the effectiveness of the use of tungsten oxide as a passivation layer. They have to be compared with rear-surface passivation of low-resistivity p-type crystalline silicon of passivated emitter and rear cell (PERC) solar cells using an Atomic-Layer-Deposited 130 nm-thick Al_2O_3 single layer, resulting in a rear surface recombination velocity as low as 90 cm/s and device efficiency as high as 20 % [38].

3.2.3. Photoluminescence

Fig. 6 depicts the photoluminescence spectra of porous silicon before and after treatment with WO_3 during different immersion times (30, 60, 300 and 360 s) for the concentration C_3. The measurement was performed in the wavelength range of 480–750 nm at room temperature. We observed an enhancement of the PL intensity of all PS/WO_3 samples. The maximum intensity was obtained for an immersion time of 360 s. It is clearly seen that coating Ps with WO_3 could protect PS from its PL intensity degradation, which may be related to the coating effect of WO_3 on PS surface chemistry. The pumping source for PL measurement was the 447 nm laser which is not the excitation wavelength of WO_3, so the PL amelioration observed is attributed to porous silicon properties changes by WO_3 deposition. This amelioration is due to the passivation of PS layer and the reduction of the surface recombination velocity. The principal peak of PS sample is blue shifted in the range of (2.11 -2.14 eV) after WO_3 treatment. We also observed the presence of a large peak around 2.4 eV. This behavior is due to WO_3 incorporation effect in the porous silicon matrix which may modify the surface electronic structure by creating new radiative centers [39]. However, for longer immersion durations, the quantity of WO_3 deposited on the porous layer promotes the non-radiative energy transfer by creating excitation energy traps.

4. Conclusion

In this work, we have reported a detailed study on the deposition effect of WO_3 thin film on a porous silicon substrate by a simple and effective dip-coating technique. FTIR results demonstrated the deposition of WO_3 layer. AFM confirmed the total coverage of porous silicon surface by WO_3 nanostructured thin film. PS/WO_3 samples exhibits a low surface reflectivity up to about 5 %. A ~ 50 % enhancement of the minority carrier lifetime by decreasing the surface recombination velocity was achieved when depositing WO_3 with an optimum 0.018 mol/L concentration of tungsten hexachloride in water/ethanol solution, which leads to an increase in the photoluminescence intensity in comparison with untreated PS layer. Obtained results confirmed that tungsten oxide is a good passivation layer to improve the porous silicon electronic an optical properties, and thus encouraging its integration in many applications such as solar cells and gas detectors. Despite these interesting results, a further amelioration of the deposited films properties is in demand. In particular, the reduction of the surface recombination velocity, the thermal treatment of dip-coated WO_3 layers or a change in the tungsten oxide deposition technique should be investigated. Further studies are in progress to test other dielectrics oxides materials to passivate porous silicon such as ALD-Al_2O_3.

Acknowledgements

The authors wish to thank Alain Ranguis of the near-field microscopy service and Vasile Heresanu from the x-rays service for measurements done at the *Centre Interdisciplinaire de Nanoscience de Marseille* (CINaM).

References

[1] J. Zhao, X. Yang, Photocatalytic oxidation for indoor air purification: a literature review, Building and Environment, 38(2003), p.645.

[2] J. Rong, T. Zhang, F. Qiu, X. Rong, X. Zhu, X. Zhang, Preparation of hierarchical micro/nanostructures Bi_2S_3-WO_3 composites for enhanced photocatalytic performance, J. Alloys Compd., 685 (2016), p.812.

[3] M.A. Gondal, M.A. Suliman, M.A. Dastageer, Gaik-Khuan Chuah, C. Basheer, Dan Yang, A. Suwaiyan, Visible light photocatalytic degradation of herbicide(Atrazine) using surface plasmon resonance induced in mesoporous Ag-WO_3/SBA-15 composite, J. Mol. Catal. A: Chem., 425 (2016), p. 208.

[4] J. Zhang, X. Suo, X. Liu, B. Liu, Y. Xue, L. Mu, H. Shi, PdO loaded WO3 COMPOSITE WITH Na2W4O13 flake: A 2-D heterostructure composite material, Mater. Lett., 184 (2016), p. 25.

[5] J. Guérin, K. Aguir, M. Bendahan, Modeling of the conduction in a WO3 thin film as ozone sensor, Sens. Actuators B., 119 (2006), p. 327.

[6] D. Li, L. Meng, S. Dang, D. Jiang, W. Shi, Hydrogen peroxide sensing using Cu2O nanocubes decorated by Ag-Au alloy nanoparticles, J. Alloys Compd., 690 (2017), p. 1.

[7] M. Rajabi, R. S. Dariani, Current improvement of porous silicon photovoltaic devices by using double layer porous silicon structure: applicable in porous silicon solar cells, J Porous Mater., 16 (2009), p. 513.

[8] F. Gourbilleau, C. Dufour, B. Rezgui, G. Brémond, Silicon nanostructures for solar cell applications, Mater. Sci. Eng. B., 159-160 (2009), p. 70.

[9] G. Conibeer, M. Green, R. Corkish, Y. Cho, E. Cho, Ch. Jiang, Th. Fangsuwannarak, E. Pink, Y. Huang, T. Puzzer, Th. Trupke, B. Richards, A. Shalav, K. Lin, Silicon nanostructures for third generation photovoltaic solar cells, Thin Solid Films., 511(2006), p. 654.

[10] B. Gelloz, A. Bsiesy, N. Koshida, Conduction and luminescent properties of wet porous silicon, J Porous Mater., 7 (2000), p. 103.

[11] H. Elhouichet, M. Oueslati, B. Bessais, H. Ezzaouia, O. Ben Younes, Laser induced degradation of photoluminescence intensity of porous silicon, J Porous Mater., 7 (1999), p. 307.

[12] L. Schirone, G. Sotgiu, F. P. Califano, Chemically etched porous silicon as an anti-reflection coating for high efficiency solar cells, Thin Solid Films., 297 (1997), p. 296.

[13] M. Jeske, J. W. Schultze, M. Thonissen, H. Munder, Electrodeposition of metals into porous silicon, Thin Solid Films., 255 (1995), p. 63.

[14] M. Ben Rabha, M. Salem, M. A. El Khakani, B. Bessais, M. Gaidi, Monocrystalline silicon surface passivation by Al_2O_3/porous silicon combined treatment, Mater. Sci. Eng. B., 178 (2013), p. 695.

[15] X.W. Du, Y. W. Lu, J. P. Liu, J. Sun, Improvement of photoluminescence properties of porous silicon by silica passivation, Appl. Surf. Sci., 252 (2006), p. 4161.

[16] M. E. Raypah, N. M. Ahmed, Characterization of porous silicon thin films passivated by a nano-silver layer, Mater. Sci. Semicond. Process., 31 (2015), p. 235.

[17] K. A. Salman, K. Omar, Z. Hassan, Effective conversion efficiency enhancement of solar cell using ZnO/PS antireflection coating layers, Solar Energy., 86 (2012), p. 541.

[18] M. Barbouche, R. Benabderrahmane Zaghouani, N.E. Benammar, V. Aglieri, M. Mosca, R. Macaluso, K. Khirouni, H. Ezzaouia, New process of silicon carbide purification intended for silicon passivation, Superlattices and microstructures. 101(2017), p. 512.

[19] T. Rahman, R. S. Bonilla, A. Nawabjan, P. R. Wilshaw, S. A. Boden, Passivation of all-angle black surfaces for silicon solar cells, Sol. Energy Mater. Sol. Cells., 160 (2017), p. 444.

[20] C. S. Blackman, I. P. Parkin, Atmospheric Pressure Chemical Vapor Deposition of Crystalline Monoclinic WO_3 and WO_{3-x} Thin Films from Reaction of WCl_6 with O-Containing Solvents and Their Photochromic and Electrochromic Properties, Chem. Mater., 17 (2005), p. 1583.

[21] C. C. Liao, F. R. Chen, J. J. Kai, Electrochromic properties of nanocomposite WO_3 films, Sol. Energy Mater. Sol. Cells., 91 (2007), p. 1282.

[22] C. Gomez-Solis, D. Sanchez-Martinez, I. Juarez-Ramirez, A. Martinez-de la Cruz, L. M. Torres-Martinez, Facile synthesis of m-WO 3 powders via precipitation in ethanol solution and evaluation of their photocatalytic activities, J. Photochem. Photobiol. A., 262 (2013), p. 28.

[23] D. F. Wang, J. R. Liang, C. Q. Li, W. J. Yan, M. Hu, Room temperature NO2 gas sensing of Au-loaded tungsten oxide nanowires/porous silicon hybrid structure, Chin. Phys. B, 25 (2016), p. 028102.

[24] R. G. Gordona, S. Barry, J. T. Barton, R.N.R. Broomhall-Dillard, Atmospheric pressure chemical vapor deposition of electrochromic tungsten oxide films, Thin Solid Films., 392 (2001), p. 231.

[25] C. P. Li, C.A. Wolden, A. C. Dillon, R. C. Tenent, Electrochromic films produced by ultrasonic spray deposition of tungsten oxide nanoparticles, Sol. Energy Mater. Sol. Cells., 99 (2012), p. 50.

[26] N. Sharma, M. Deepa, P. Varshney, S.A. Agnihotry, FTIR and absorption edge studies on tungsten oxide based precursor materials synthesized by sol–gel technique, J. Non-Cryst. Solids., 306 (2002), p. 129.

[27] A. J. More, R. S. Patil, D. S. Dalavi, S. S. Mali, C. K. Hong, M. G. Gang, J. H. Kim, and P. S. Patil, Electrodeposition of nano-granular tungsten oxide thin films for smart window application, Mat. Lett., 134 (2014), p. 298.

[28] M. Regragui, M. Addou, A. Outzourhit, J. C. Bernede, E. El Idrissi, E. Benseddik, and A. Kachouane, Preparation and characterization of pyrolytic spray deposited electrochromic tungsten trioxide films, Thin Solid Films., 358 (2000), p. 40.

[29] J. Malm, T. Sajavaara, M. Karppinen, Atomic layer deposition of WO_3 thin films using $W(CO)_6$ and O_3 precursors, Chem. Vap. Deposition., 18 (2012), p. 245.

[30] S. Badilescu, P. V. Ashrit, Study of sol-gel prepared nanostructured WO_3 thin films and composites for electrochromic applications, Solid State Ionics., 158 (2002), p. 187.

[31] I. Haddadi, W. Dimassi, R. Bousbih, M. Hajji, M. A. Kanzari, H. Ezzaouia, Improvement of solar cells performances by surface passivation using porous silicon chemically treated with LiBr solution, Phys. Status Solidi C., 6 (2011), p. 1837.

[32] J. Diaz-Reyes, V. Dorantes-Garcia, A. Pérez-Benitez, J. A. Balderas-López, Obtaining of films of tungsten trioxide (WO3) by resistive heating of a tungsten filament, Superf. vacio., 21 (2008), p. 12.

[33] M. Deepa, M. Kar, S. A. Agnihotry, Electrodeposited tungsten oxide films: annealing effects on structure and electrochromic performance, Thin Solid Films., 468 (2004), p. 32.

[34] N. Mendoza-Aguero, V. Agarwal, Optical and structural characterization of tungsten oxide electrodeposited on nanostructured porous silicon: Effect of annealing atmosphere and temperature, J. Alloys Compd., 581 (2013), p. 596.

[35] M. Atyaoui, W. Dimassi, M. Khalifa, R. Chtourou, H. Ezzaouia, Improvement of photoluminescence and electrical properties of porous silicon layer treated with lanthanum, J. Lumin., 132 (2012), p. 2572.

[36] S. Rein, Lifetime Spectroscopy, ISBN-10 3-540-25303-3, Springer Berlin Heidelberg New York (2004).

[37] S. Aouida, N. Bachtouli, B. Bessais, Light induced enhancement of minority carrier lifetime of chemically passivated crystalline silicon, Appl. Surf. Sci., 274 (2013), p. 255.

[38] J. Schmidt, A. Merkle, R. Brendel, B. Hoex, M. C. M. Van de Sanden, W. M. M. Kessels, Surface passivation of high-efficiency silicon solar cells by atomic-layer-deposited Al_2O_3, Prog. Photovolt: Res. Appl. 16 (2008), p. 461.

[39] M. B. Bouzourâa, M. Rahmani, M. A Zaïbi, N. Lorrain, L. Hajji, M. Oueslati, Optical study of annealed cobalt-porous silicon nanocomposites, J. Lumin. 143 (2013), p. 521.

Figure captions

Fig. 1: FTIR absorption spectra of (a) PS and PS/WO_3 samples (b) amplification of zone 2 for PS sample (c) amplification of zone 2 for PS/WO_3 sample (d) amplification of zone 3 for PS sample (e) amplification of zone 3 for PS/WO_3 sample

Fig. 2: AFM image of (a) untreated porous silicon surface (b) porous silicon surface covered with WO_3 for an immersion time of 360 s in WCL_6 solution (c) Top surface SEM view of porous silicon surface covered with WO_3 for an immersion time of 360 s in WCL_6 solution.

Fig. 3: (a) Reflectivity spectra of PS and PS/WO_3 samples with different immersion times (b) Reflectivity spectra of PS sample and untreated silicon substrate.

Fig. 4: Effective minority carrier lifetime as a function of excess carrier density of untreated silicon, PS and PS/WO_3 samples for different concentration C_1=0.086 mol/L, C_2=0.035 mol/L and C_3=0.018 mol/L for an immersion time of 30 s.

Fig. 5: (a) Effective minority carrier lifetime as a function of excess carrier density of untreated silicon, PS and PS/WO_3 samples for different immersion times and a concentration C_3=0.018 mol/L (b) Effective Surface recombination velocity S_{eff} as a function of immersion time

Fig. 6: PL spectra of PS and PS/WO_3 samples with different immersion times for the concentration C_3=0.018 mol/L performed at room temperature using 447 nm blue-violet laser diode and 475 nm long pass edge filter.

Figure 1

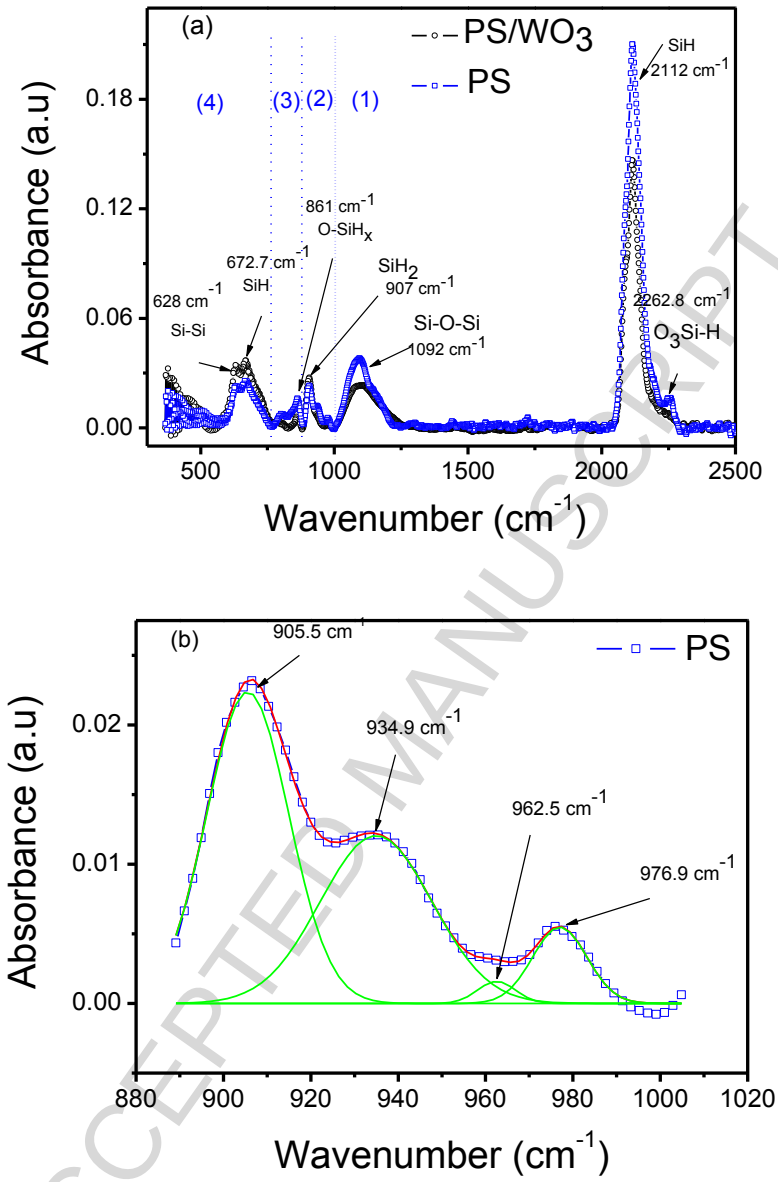

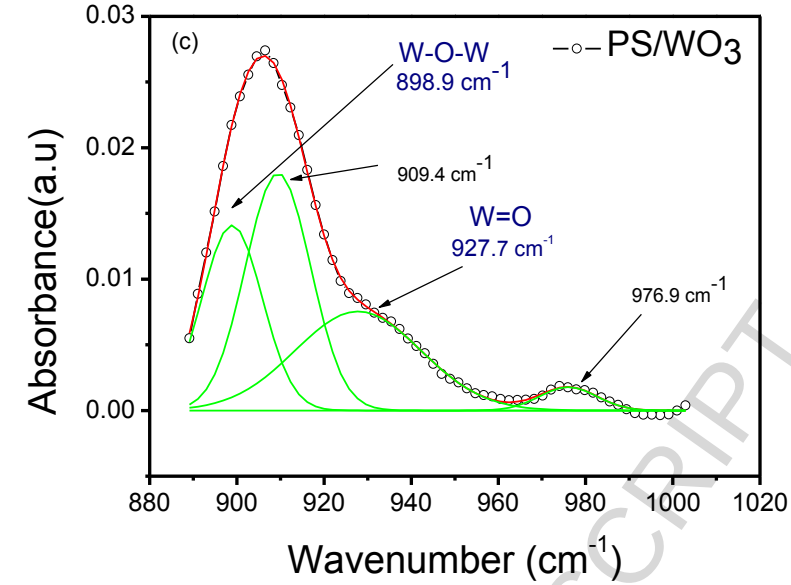

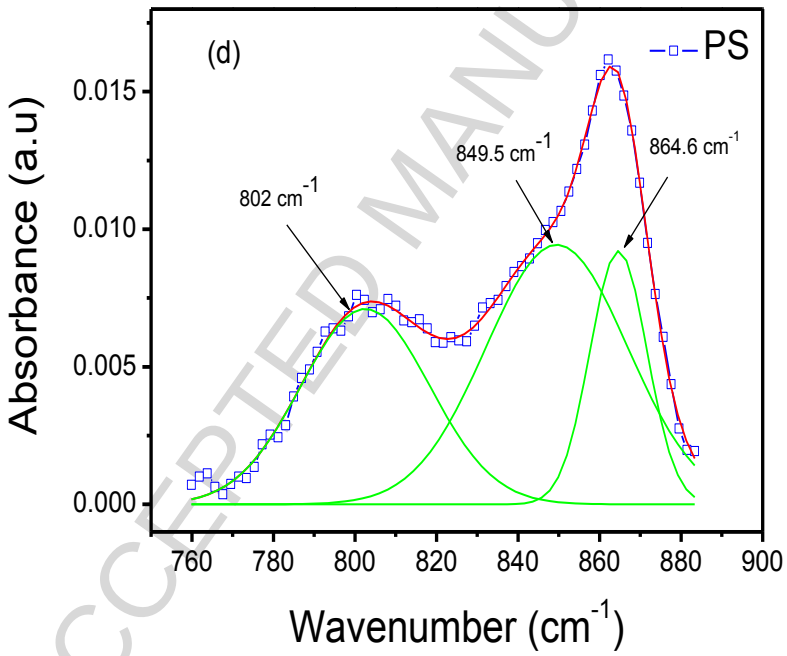

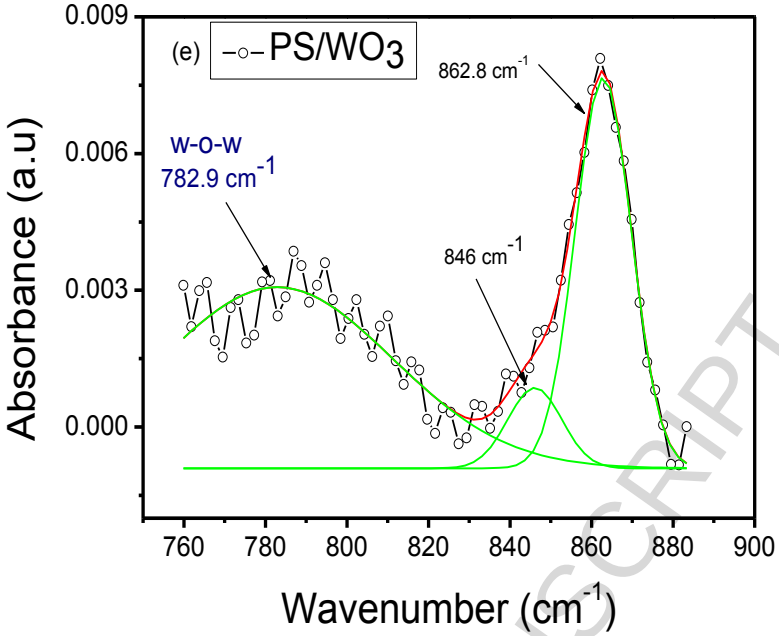

Figure 2(a)

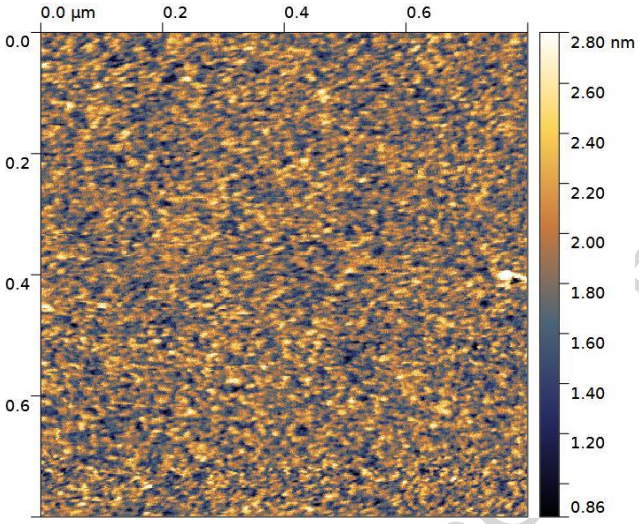

Figure 2(b)

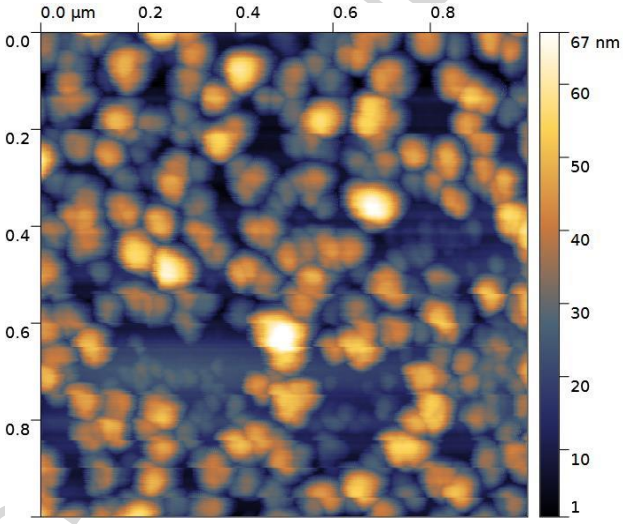

Figure 2(c)

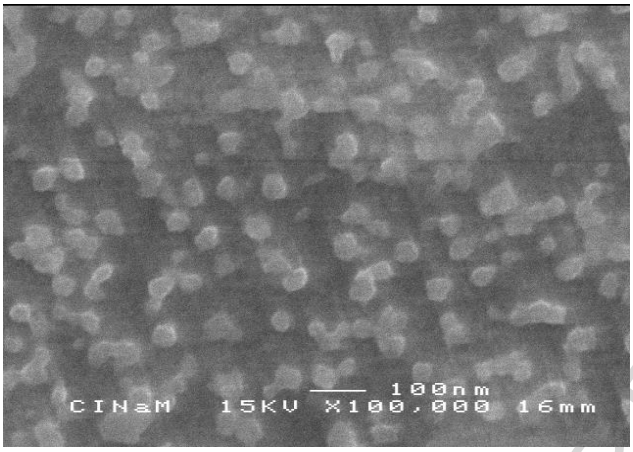

Figure 3(a)

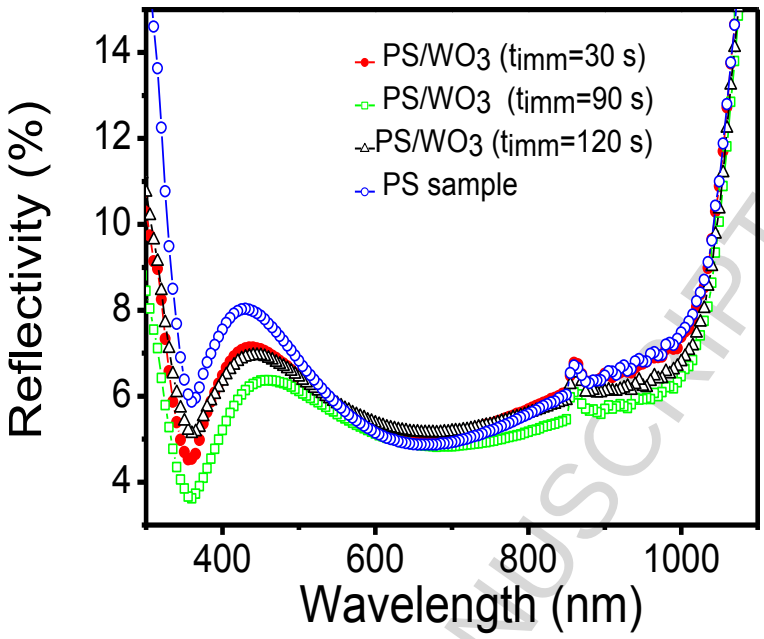

Figure 3(b)

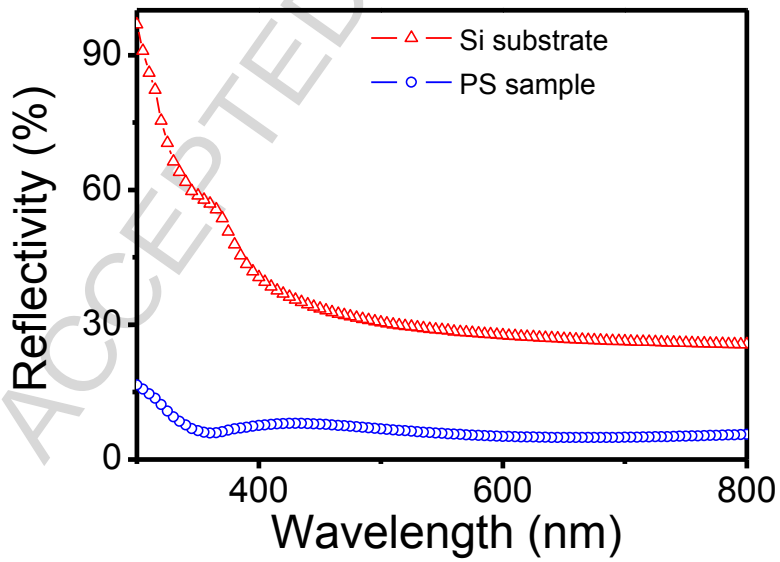

Figure 4

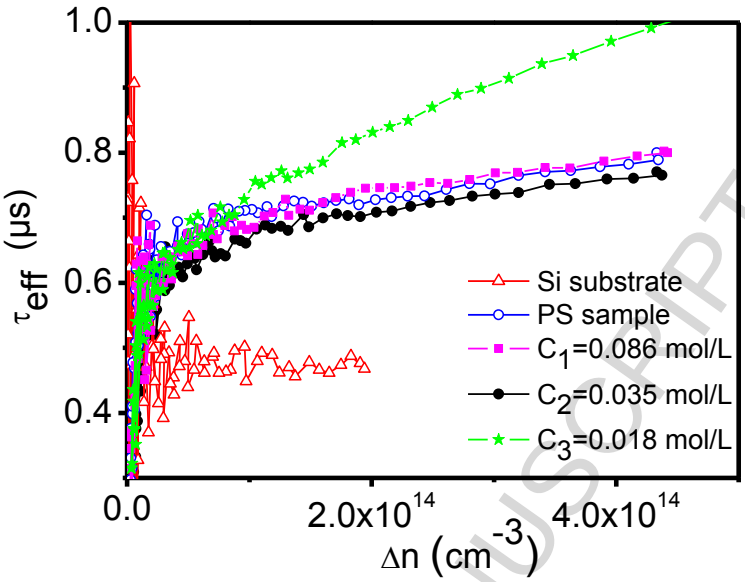

Figure 5 (a)

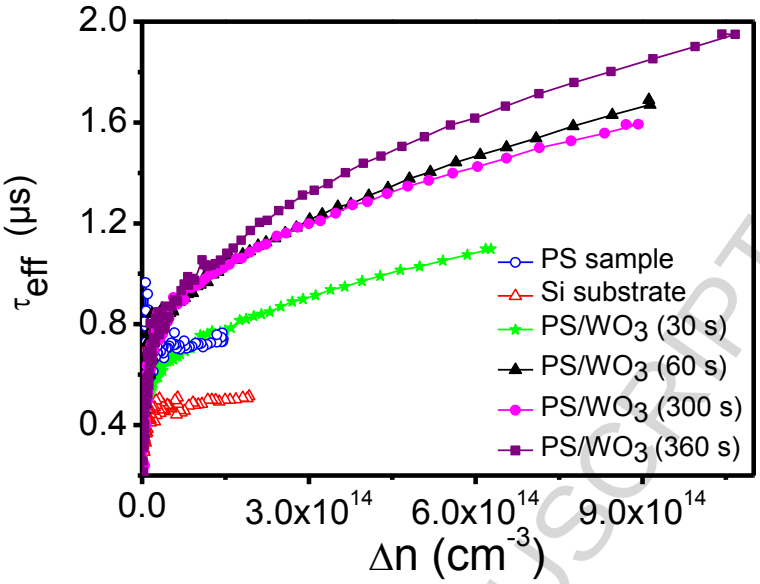

Figure 5 (b)

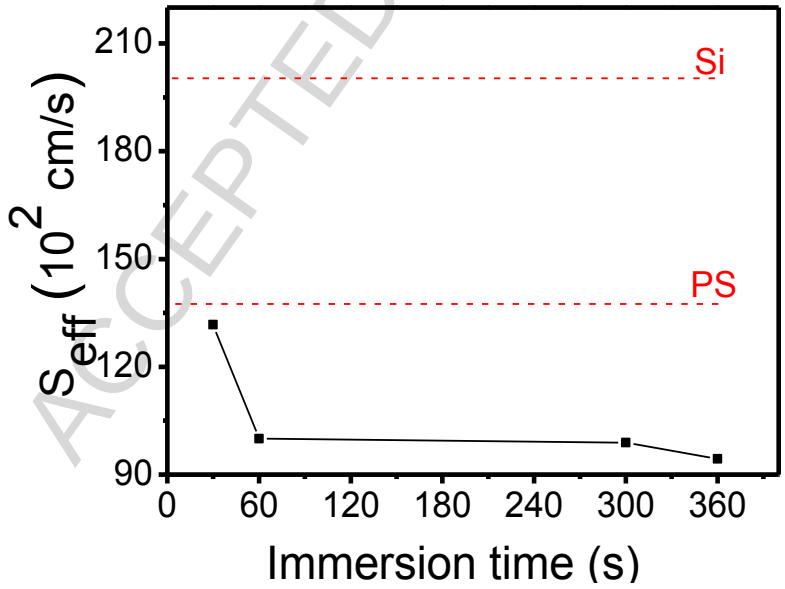

Figure 6

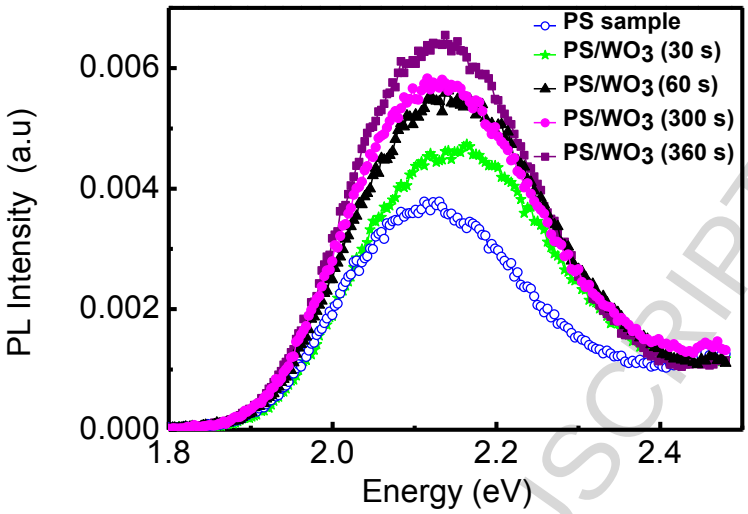

Highlights:

- Deposition of Tungsten trioxide on porous silicon surface.
- Enhancement of carrier lifetime and surface recombination velocity.
- Increase of the photoluminescence of elaborated samples.